

## BEHAVIOR OF SHALLOW-DEPTH COMPOSITE BEAMS WITH ALTERNATIVE SHEAR CONNECTORS

By Christopher Higgins<sup>1</sup>

**Abstract:** Experimental tests of composite (concrete/steel) beams with alternative shear connectors were performed. The shallow-depth specimens consisted of steel WT-sections composite with a concrete slab. Differing degrees of composite action were achieved by shear connectors consisting of concrete filled holes located in the webs of the steel WT-sections and friction along the embedded stem. Static test results indicated that differing levels of composite action can be achieved and depend on the number and type of shear connectors. Connector capacity was estimated and compared with available models. Member capacities were compared with factored design moment requirements for a bridge deck application.

### INTRODUCTION and BACKGROUND

Concrete combined with structural steel shapes are widely used in structural engineering to provide composite structures. These structures make use of the best attributes of the component materials: tensile strength of structural steel and compressive strength of concrete. Composite action between concrete and steel elements is generally accomplished using headed shear studs although other mechanical connectors such as welded structural steel plates, bars, and channels, as well as reinforcing steel are also used.

An alternative type of shear connector called a Perfobond Strip, or more generally a plate rib shear connector, has been studied in Japan, Europe, Canada, Australia, and the United States. The connector has several forms, but typically consists of a steel plate with holes that is welded to

---

<sup>1</sup> Assistant Professor, Dept. of Civil Engineering, Oregon State University, Corvallis, OR 97331.

the top flange of a steel girder. When concrete is cast, the holes in the steel plate are filled with the fresh concrete. After the concrete cures, the combined action of end bearing of the plate on the concrete, shear strength of concrete dowels (concrete filled holes in steel plate), and friction enables shear transfer between the steel and concrete slab. Research on plate rib shear connectors has been conducted for both bridge (Nishimura *et al.* 1971)(Zellner 1987)(Leonhardt *et al.* 1987)(Roberts and Haywood 1995) and building construction applications (Medberry and Shahrooz 2002)(Oguejiofor and Hosain 1992)(Velandia and Hosain 1992)(Oguejiofor and Hosain 1994). Reported advantages of this type of shear connector are negligible slip under service load, fabrication cost savings, and improved safety due to reduced trip hazard during construction. Much of the previous research has focused on composite beams, typical of floor joists or stringers. Recently the connectors have been studied for application to bridge decks (Higgins and Mitchell 2002).

Assessment of plate rib shear connectors has generally been performed using push-through specimens that do not reflect realistic stress-states and load-transfer mechanisms, or on moderately large and deep steel beams with end bearing on the connectors. To assess the behavior of plate rib shear connectors for shallow depth flexural elements (decks) with connectors continuously distributed along the embedded steel shape and no end bearing, a series of experiments was conducted. Beam specimens with several alternative hole configurations and spacings were investigated and different steel shapes and reinforcements were studied.

## **EXPERIMENTAL PROGRAM**

### **Specimen Description**

A series of beam tests were performed to assess the flexural behavior of shallow depth composite beams employing continuous plate rib shear connectors. Specimens consisted of full-

sized prototype beams representative of a strip from a bridge deck having orthotropic properties (Higgins and Mitchell 2002). Beams specimens were constructed from a hot-rolled WT shape cast integrally with a reinforced concrete slab element as illustrated in Fig. 1. Two WT shapes of A572-Grade 50 steel were investigated including WT4x5 and WT5x6. To provide similar cross-sectional properties for the two different WT shapes, the web of the WT5x6 was embedded into the slab an additional 25mm (1 in) as shown in Fig. 1. The concrete element consisted of a 203mm wide by 112mm thick (8 in x 4.5 in) slab. Reinforcing steel was 16mm bars (#5) spaced 152 mm (6 in.) on-center in the longitudinal direction and 8 mm (#2) and 10 mm bars (#3) spaced alternatively 102 mm (3 in.) on-center in the transverse direction. The amount of transverse steel placed in the specimens was larger than the amount used in an actual deck and was added to prevent concrete splitting over the web of the embedded WT-section. In an actual deck, additional lateral confinement is provided by adjacent concrete. Transverse reinforcement was placed through the web perforations in only two specimens. The remaining specimens were constructed with the transverse reinforcement located on top of the WT webs. The concrete mix used for the slab was the New York State Department of Transportation "Class DP mix" with aggregate gradation CA-1. This corresponds to a maximum aggregate size of 25 mm (1 in.) with 90 to 100% passing 13 mm (0.5 in.) and 0 to 15% passing 6 mm (0.25 in.). Concrete compressive strength at the time of testing was 39.3 MPa (5770 psi).

Connection between the steel WT and concrete slab was made using different perforation shapes including closed circular holes, circular holes made at the edge of the web which produce C-shapes perforations, and U-shaped perforations (Fig. 1). All perforations were made by punching through the steel WT-beam web. Circular and C-shaped perforations were made from 19mm (0.75 in) diameter dies. The U-shaped perforation was made from 19mm diameter half-circle at the bottom of the U. Several different perforation spacings were also investigated. After

curing, the concrete filled perforations combined with friction along the embedded portion of the WT web provide shear transfer between the steel and concrete. To eliminate chemical bond between the WT and concrete slab and reduce friction along the steel/concrete interface, a thick coating of white lithium grease was applied to WT webs for all but four specimens. Specimens with grease applied to the web and with holes spaced at 305 mm (12 in.) (SC12GN, TC12GN) were designed to provide the lowest degree of composite action (simulating noncomposite behavior). Specimens with rebar through the holes (SC3GR, TC3GR) were designed to provide the highest degree of composite action (simulating fully-composite behavior).

#### **Test Scope and Test Designations**

This study involved shallow depth composite beams constructed with different hot-rolled WT shapes, web perforation types, web perforation spacing, reinforcing steel located in the perforations, and friction along the WT web embedded in the concrete slab. The nomenclature used to designate different specimens is shown in Fig. 2 and the complete test matrix is shown in Table 1. Material properties for the reinforcing steel and concrete used to construct the specimens are shown in Table 2.

#### **Testing Procedure**

After curing, beams were placed on roller supports and subjected to four-point bending as shown in Fig. 3. Overall span for the specimens was 2.29 m (7.5 ft). A 1.3 MN (300 kip) capacity hydraulic cylinder attached to a reaction frame was used to load the specimens. A stiffened W12x24 spreader-beam resting on 51 mm (2 in.) diameter steel rollers spaced at 457mm (18 in) provided a constant moment region at midspan. Directly under the rollers, steel plates were used to prevent local crushing of the concrete. Hydrostone under these plates provided uniform contact on the concrete surface. Instrumentation consisted of strain gages, concrete clip gages,

displacement transducers, and a load cell placed in series with the hydraulic cylinder. Strain and clip gages were used to assess the local concrete and steel strains as well as the slip strains at three locations on the cross section. Displacement transducers, located at the level of the web perforations, measured the amount of relative slip between the WT and concrete slab at ends of the beam. Data from sensors were acquired using a PC-based data acquisition system and were continuously sampled at a rate of 1 hz during the tests.

Specimens were subjected to slowly applied monotonic load from the hydraulic cylinder using a manual hydraulic pump. Specimens were initially loaded into the elastic range and then unloaded to ensure that instrumentation and data acquisition systems were functioning properly. After elastic loading and unloading, specimens were loaded to failure. Several specimens were also unloaded after the onset of significant slip between the WT and concrete slab to assess unloading and reloading behavior. During tests, loading was suspended to observe and record concrete cracking and specimen condition.

## **TEST RESULTS**

All specimens failed by crushing of the concrete near midspan. However, the degree of composite action achieved between the concrete and WT-shape significantly affected the overall behavior of the beams. Test results are summarized in Table 4 and Moment-displacement relationships at midspan for several of the specimens are shown in Figs. 4a-e. From these figures, key differences in behavior can be observed. Specimens with few widely spaced connectors (Fig. 4a) begin to soften at relatively low moment and had reduced strength and large displacements at failure. Additional friction along the concrete-web interface permitted the specimens without grease on the WT-web to achieved higher moment capacity and larger secant stiffness as compared to ungreased specimens (Fig. 4b). Additional surface area at the concrete-web interface

for the WT5x6 specimens enabled higher capacity than equivalent WT4x5 specimens (Figs. 4b and 4c). No significant difference was observed for initial stiffness between equivalent WT5x6 and WT4x5 specimens (Fig. 4c). The contribution of friction along the web-concrete interface did not become significant until after slip initiation at the end of the beam and the frictional contribution to maximum moment is more significant for specimens with few connectors that slip at low loads (Fig. 4b). Specimens with different hole shapes exhibited similar initial stiffnesses but U and C-shaped holes achieved higher moment before softening (Fig. 4d). The U and C-shaped holes have larger concrete areas that are also located higher into the concrete slab, which provides additional confinement to the connectors. U and C-shaped holes also have sharp edges located at the top of the stem that can scrape against the concrete slab as slip occurs, permitting additional shear transfer. Placing reinforcing steel through the holes did not alter the initial stiffness, but did permit these specimens to achieve larger moment capacity (Fig. 4e).

Flexural cracking of the concrete was observed at lower moment magnitude for specimens with lesser degrees of composite action (approximately 12.2 kN-m (108 kip-in) for SC12GN compared to 36.6 kN-m (324 kip-in) for SC3GR). Cracking of the concrete deck parallel to the WT-stem was observed in only one specimen (at the east end of SO2GN) and appeared as the beam achieved the failure load. The crack extended to the top of the WT-web and then turned parallel to the slab soffit. No other splitting cracks were observed. Concrete spalling at web-hole locations was observed adjacent to the supports for WT4x5 specimens (S designation) after significant slip between the concrete and steel and occurred well after the peak moment was achieved. No spalling was observed for the WT5x6 specimens (T designation), as these holes were located higher into the concrete slab. No vertical separation between the concrete and WT was observed during testing.

Varying degrees of composite action between the concrete slab and steel shape were achieved through the combination of concrete filled holes in the WT-webs and friction along the web embedment. The effectiveness of the shear transfer mechanisms was assessed using the measured concrete strains combined with bottom flange and web strains in the WT at three different locations along the span. Measured strains were compared with those for theoretical noncomposite and fully-composite beams. Theoretical moment-strain behavior, shown in Fig. 5a, for ideally noncomposite and fully-composite beams were determined assuming no vertical separation between the concrete and steel, concrete and steel have identical curvatures at points along the beam, steel exhibits elastic-perfectly plastic behavior, concrete contributions in flexural tension can be neglected, and concrete material behavior in compression is represented by a continuous constitutive rule (Todoshini *et al.* 1964). The ultimate concrete strain was selected as 0.003, which is consistent with practice and with the observed specimen concrete strains at crushing. Slip strain was computed as the difference between the concrete and steel strains where these elements overlap. Comparison between the ideal cases clearly shows the larger ultimate moment that can be achieved if slip between the steel and concrete components is minimized. Measured strains on the cross section at midspan for a range of specimens is shown in Figs. 5b-d. Slip strain was computed by subtracting the actual measured concrete strain from the predicted concrete strain based on measured steel strains in the WT (web and flange). For all specimens, concrete and steel strains initially increased linearly as the load increased. This is consistent with behavior for a composite cross section where the concrete strain gage, located above the neutral axis, indicated compression (negative values of strain) and both the web and flange strain gages, located below the composite neutral axis, indicated tension (positive values of strain). However, as the applied load continues to increase, the web strain gage begins to reverse and eventually becomes compressive for some specimens (SC12GN). This indicates that the shear transfer mechanism between the concrete and WT deteriorates and the degree of composite action is

reduced by virtue of a discontinuity in the strains (plane sections no longer remain plane). Once the web strains begin to reverse direction, the slip strains increase rapidly and the section begins to indicate two neutral surfaces: one in the concrete and one in the WT section. The more negative the web strain, the lower the composite action in the beam. By comparison, the web strain in specimen SC3GN remains in tension at ultimate indicating a higher degree of composite action.

Example slip strain distributions along the length of the beam at varying load stages are shown in Fig. 6. Slip strains were assumed to be constant between the loading points and equal to the value measured at midspan. Slip displacements at hole-connector locations were determined by integrating the slip strains along the length of the beam. Actual measured end-slip displacements at the ends of a specimen are shown in Fig. 7. As loading begins, both ends exhibit similar slip displacement magnitudes and little slip occurs. However, as the maximum moment is achieved, the slip increases at one end and becomes much larger than the other. This is reflected in the slip strain distribution where slip strains on the left hand side correspond to the east end of the beam. Comparison between calculated end-slip displacement (determined by integrating slip strains) and the measured end-slip displacement indicates that integration of the slip strains tended to underestimate the experimentally measured end-slip displacements. Accuracy may be improved by instrumenting additional cross-sections to better characterize the slip-strain distribution along the length of the beam.

Moment-curvature response was determined for each of the specimens and compared with the theoretical response for fully-composite and noncomposite beams. Experimental curvature at a cross-section was determined from the gradient in the WT strain measurements on the web and flange at midspan. Complete moment-curvature relationships could be determined for the WT4x5 as shown in Fig. 8. However, complete moment-curvature relationships for WT5x6

specimens could not be developed due to large increases in flange strains measured at the onset of yielding. Comparison of measured and theoretical responses indicated that specimens with connector spacing less than 305 mm (12 in.) exhibited response similar to that of the fully-composite beam up to a moment of at least 31.6 kN-m (280 kip-in). Several specimens exhibited moment-curvature response similar to the theoretical fully-composite beam up to much higher loads. The specimen with reinforcing steel passing through the holes (SC3GR) achieved similar moment capacity to the theoretical fully-composite beam. Few widely spaced connectors were closer to the ideal non-composite beam.

Concrete filled connectors and friction permit transfer of shear force between the concrete slab and steel section. The sum of these connector forces in the first 457 mm (18 in) length of beam from the support to the location of the first series of strain gages (Fig.3) was determined by computing the axial force in the WT using strain gage measurements. If there were no composite action in the beam, the net axial force in the WT would be zero. The total connector force is shown relative to the measured end-slip displacement in Fig. 9. As shown in this figure, the connectors are initially stiff and exhibit gradual softening until the end-slip displacement reaches approximately 0.8 mm (0.03 in) and then the force begins to diminish. The observed response is an example of rigid limited-slip capacity shear connectors. Experimentally determined horizontal shear was compared with the theoretical shear as illustrated in Fig. 10. As seen in this figure, specimens with rebar through the holes and with U shaped perforations, exhibited horizontal shear close to the theoretical until the maximum moment. The specimens with widely spaced holes deviated from the theoretical behavior at relatively low loads.

Individual connector forces were not possible to determine from the instrumentation placed on the specimens. However, an average connector force was determined by dividing the

axial force measured in the WT as determined above by the number of concrete connectors within the length of beam from the support to the first set of strain gages. Only specimens with greased steel-concrete interfaces and without rebar through the holes were used in this assessment. The stress in each connector was determined by dividing the average connector force by the area of concrete at the steel-concrete perforation interface. The O shaped perforations had concrete shearing planes on the two web faces corresponding to the area of the individual holes, while C and U shaped holes had an additional concrete shear plane associated with the top of the WT stem. The maximum connector stress values are summarized in Table 5 and shown in Fig. 11. Based on measured slip-strain distributions (Fig. 6), the slip-displacement varied nonlinearly along the length of the beam as the moment increased. Thus, connectors located at the ends of the beam were subject to larger demand. When these connectors exceed their slip capacity they begin to unload, while others, subjected to smaller slip displacements continue to carry larger loads. This interaction results in the observed softening behavior. Eventually, as slip displacements become large enough along the beam, all connector forces within the span begin to erode and finally reach a terminal sliding frictional force distributed along the concrete-steel interface. This terminal sliding friction force remained nearly constant at approximately 68 N/mm (389 lbs/in) of length (SC12GN Fig. 9). The shearing stress on the concrete connectors was estimated by computing the horizontal shear force produced between the end-support and the first set of strain gages (457 mm (18 in.) long portion of the specimen). The horizontal force value produced for the greased S and T specimens with 305 mm (12 in.) connector spacing was subtracted from the other greased specimens using the same WT shape to conservatively remove the steel-concrete friction contribution along the web-slab interface. The remaining horizontal force was attributed to the shear planes of the concrete filled perforations in the WT web. The average concrete connector shear stress was computed by dividing the remaining horizontal force by the total concrete area on the shear planes within the 457 mm (18 in.) length of specimen as seen in Table 5. The average

concrete stress was 15.9 MPa (2300 psi). An ultimate connector concrete shear stress  $f_{cvu}$  (psi) was determined as a function of the concrete compressive strength as:

$$f_{cvu} = 30\sqrt{f'_c} \quad [1]$$

where  $f'_c$  is the compressive strength of the concrete (psi) and 30 is an empirical coefficient determined from test results for specimens with greased webs (to minimize the steel-concrete frictional contribution) and without rebar through the holes. If the smallest measured value from all tests is taken as the limit, the empirical coefficient becomes 17. The force for each connector can be determined as:

$$F_{cu} = 30A_{cv}\sqrt{f'_c} \quad [2]$$

where  $A_{cv}$  the total concrete area in the shear planes for a given web perforation. Previous research has developed connector shear force capacity equations based on subassembly tests, such as push-through and shear-box specimens. Leonhardt *et. al.* (1987) used push-through specimens prevented from end-bearing of the connector plate on the concrete and with rebar through some of the holes to predict the connector capacity as:

$$F_{cu} = 1.6A_{cv}f'_c \quad [3]$$

where the coefficient 1.6 is in-place of the original 1.3 to adjust for the North American practice of using cylinder strengths instead of cube strengths. Oguejiofor and Hosain (1994) performed push-through specimens having end-bearing of the connector plate and predicted connector capacity as:

$$F_{cu} = 22.01A_{cv}\sqrt{f'_c} \quad [4]$$

Roberts and Heywood (1995) used individual concrete filled holes in shear boxes with various confining forces on the shear planes predicted connector capacity as:

$$F_{cu} = 25.29A_{cv}\sqrt{f'_c} \quad [5]$$

where this a simplified form of the original equation by neglecting higher order terms that do not contribute significantly for the geometry considered. Finally, Medberry and Shahrooz (2002) performed push-through tests of specimens having end-bearing of the connector plate and predicted connector capacity as:

$$F_{cu} = 10A_{cv}\sqrt{f'_c} \quad [6]$$

For the four other methods considered (Eqs. 3-6), only the concrete area in the shear planes was considered for the contribution to connector capacity because frictional contributions, end-bearing, and confining force effects were quite different for the various tests from other researchers. Comparing connector capacity from concrete in the shear planes of the specimens reported here, the connector force was in the range of those described by subassemblage tests (with the exception of Leonhardt *et al.* (1987) which included reinforcing through the holes). The proposed connector capacity (Eq. 2) is larger than those from Eq. 4 and 6 as those specimens had end-bearing of the connector plates on the concrete slab and many failures were attributed to splitting of the concrete slab that was not observed for the test specimens reported here.

### **Application for Partially-Filled Grid Bridge Deck**

The specimen configuration tested could be considered a finite slice of a partially-filled grid bridge deck composite with a concrete slab. These deck systems consist of a steel grid with main bars corresponding closely to the size of the WT used in this test program. In an actual deck application, there are also steel bars oriented perpendicular to the main bars. A concrete slab is made composite with the grid using shear connectors. Slab thicknesses used in practice correspond closely to that used in this test program. The magnitude of moment carried by the deck in strong direction (equivalent to the direction tested) depends on the relative stiffness of the deck in the two orthogonal directions and the orientation of the grid relative to the direction of traffic. Design moment equations are provided in the American Association of State Highway and Transportation Officials (AASHTO) LRFD Specification (AASHTO LRFD 2002) for decks of this type. Considering the two common cases; main bars oriented transverse to traffic and main bars oriented parallel to traffic, the largest factored moment is 76.7 kN-m/m (17.3 kip-in/in). This moment is produced for a 2.3m (7.5 ft) span when main bars are oriented parallel to traffic and considering the highest stiffness ratio recommended in the Specification (relatively low stiffness in transverse direction). Multiplying the unit factored moment by the 203 mm (8 in.) wide design strip (which corresponds to the width of tested specimens) produces a factored design moment of 15.6 kN-m (138 kip-in). Comparing the moment behavior of the test specimens, all specimens were able to achieve this level of capacity and all exhibited negligible slip at this moment magnitude except for the specimens with very widely spaced connectors (SC12 and TC12 specimens with 305 mm (12 in.) connector spacing). This indicates that many of the connector configurations investigated would be capable of providing sufficient horizontal shear capacity to develop the factored design moment strength for the cross-section and span length considered.

## Summary and Conclusions

Full-scale tests of shallow depth beams with continuously distributed alternative shear connectors have been conducted. Static tests were performed on specimens with different connector shapes, spacings, reinforcing, and steel/concrete interfaces, as well as structural steel WT shapes. Based on test results and comparisons with theoretical response, the following observations and conclusions are presented:

1. Specimens were able to develop different degrees of composite action between the concrete slab and steel WT section depending on connector shape, spacing, reinforcing, and steel-slab interface at the web.
2. In general, larger concrete areas along the shear planes between the slab and steel web increased the degree of composite action and correspondingly increased the capacity of the section.
3. Rebar placed through the holes of the shear plane between the concrete and steel web developed the highest capacity. Performance of these specimens was close to that predicted for an ideally composite beam.
4. C and U shaped perforations exhibited higher capacity than similarly spaced round connectors. This is attributed to the additional shear plane at the top of the web and a larger degree of confinement from the shear planes being located farther away from the free edge of the slab.
5. Initial specimen behavior approximated the theoretical ideally composite moment-curvature until composite action was gradually lost.
6. Composite action was gradually lost as the concrete slab begins to slip relative to the steel section upon failure of the concrete connectors crossing the shear planes closest to the ends. Global member response tended to be quite ductile for specimens with lower

levels of composite action. The failure mode for all specimens corresponding to crushing of the concrete.

7. Slip strains were symmetrical about the center of the beam at early stages of loading. As composite action was lost, the slips strains became unsymmetrical, resulting in increased slip displacement at one end of the specimen. Integration of slip strains tended to underestimate actual end displacements, due to the limited number of instrumented cross-sections.
8. Grease applied to the concrete slab-steel WT web interface reduced the degree of composite action for otherwise similar specimens. Specimens with greased webs were conservatively used to determine the connector force capacities and frictional contribution attributed to the greased web-slab interface was removed to isolate the concrete contribution along the shear planes of the web perforations. Concrete connector capacity was calculated based on the measured horizontal shear developed between the concrete slab and steel WT sections. An equation describing the connector capacity was in the range of others found in the literature.
9. All the connector configurations investigated were sufficient to develop the required AASHTO LRFD factored design moment for a partially-filled grid deck composite with a concrete slab for the test span and section properties considered. All but the four specimens with very widely spaced perforations would exhibit negligible end slip at the specified factored design moment.

#### **Acknowledgments**

Financial support for this research was provided by Exodermic Bridge Deck Inc. of Lakeville, Connecticut. Messrs. Heath Mitchell and Carl Rode provided valuable assistance in constructing and testing the laboratory specimens. The opinions, findings, and conclusions are those of the author and do not necessarily reflect the views of the sponsors or the individuals acknowledged.

## References

- American Association of State Highway and Transportation Officials (AASHTO) (2002). "LRFD Bridge Design Specifications," 2<sup>nd</sup> Edition, AASHTO, Washington, D. C.
- Higgins, C. and Mitchell, H. (2001) "Behavior of Composite Bridge Decks with Alternative Shear Connectors," *ASCE Journal of Bridge Engineering* Vol. 6(10): 17-22.
- Leonhardt, E. F., Andra, W., Andra, H-P., and Harre, W. (1987). "New Improved Shear Connector with High Fatigue Strength for Composite Structures," (in German) *Benton-Und Stahlbentonbau*, Vol. 12, 325-331.
- Medberry, S.B. and Shahrooz, B.M. (2002). "Perfobond Shear Connector for Composite Construction," *Engineering Journal*, Vol. 39(1), 2-12.
- Nishimura, A., Okumura, T., and Ariga, Y. (1971). "Shear Connector Utilizing the Reinforcing Steels in Composite Girder Slab," *Proceedings of the Symposium on New Techniques in the Construction of Structures*, 17<sup>th</sup> National Symposium on Bridge and Structural Engineering, Japan Society for the Promotion of Science, Tokyo, Japan, 35-47.
- Oguejiofor, E. C. and Hosain, M. U. (1992). "Behavior of Perfobond Rib Shear Connectors in Composite Beams: Full-Size Tests," *Canadian Journal of Civil Engineering*, Vol. 19, 224-235.
- Oguejiofor, E. C. and Hosain, M. U. (1994). "A Parametric Study of Perfobond Rib Shear Connectors," *Canadian Journal of Civil Engineering*, Vol. 21, 614-625.
- Roberts, W., and Heywood, R. (1995). "Development and Testing of a New Shear Connector for Steel Concrete Composite Bridges," Fourth International Bridge Engineering Conference, National Academy Press, Washington, D.C., 137-145.
- Todeshini, C. E., Bianchini, A. C. and Kesler, C.E. (1964). "Behavior of Concrete Columns Reinforced with High Strength Steels," *ACI Journal, Proceedings* V. 61, No. 6, pp. 701-716.
- Velanda, M. R. and Hosain, M. U. (1992). "Behavior of Perfobond Rib Shear Connectors: Push-Out Tests," *Canadian Journal of Civil Engineering*, Vol. 19, 1-10.
- Zellner, W. (1987). "Recent Designs of Composite Bridges and a New Type of Shear Connectors," *Composite Construction in Steel and Concrete*, Proceedings of an Engineering Foundation Conference, New England College, NH, 240-252.

Table 1: Dimensions to Block-outs					
Spacing		Distance 'A'		Distance 'B'	
of Holes		mm	(in)	mm	(in)
51	(2)	483	(19)	940	(37)
76	(3)	495	(20)	876	(35)
305	(12)	559	(22)	914	(36)

Table 2: Material Properties

Component	Fy		Fu		f'c	
	MPa	(ksi)	MPa	ksi	MPa	(psi)
W4x5	451	(65.4)	599	(86.9)	-	-
W5x6	405	(58.7)	526	(76.3)	-	-
#5 Rebar	440	(63.8)	668	(96.9)	-	-
#3 Rebar	476	(69.1)	758	(110.0)	-	-
Concrete	-	-	-	-	39.3	(5700)

Table 3: Theoretical Section Properties

Component	EI		First Yield Moment		Ultimate Moment	
	MPa	(kip-in <sup>2</sup> )	kN-m	(kip-in)	kN-m	(kip-in)
W4x5 Noncomposite*	14348	(127000)	10.6	(94.2)	18.5	(163.6)
W4x5 Fully Composite#	105410	(933000)	44.1	(390.0)	57.1	(505.0)
W5x6 Noncomposite*	21579	(191000)	12.3	(108.5)	23.7	(210.0)
W5x6 Fully Composite#	109364	(968000)	46.2	(409.0)	55.6	(492.0)

# Bottom flange yields first

\* Top of web yields first

Table 4: Specimen details and test results.

Specimen ID	WT Size	Hole Shape	Hole Spacing (in)	WT Web Condition	Rebar In Holes	Total Area of Concrete Shear Planes (in <sup>2</sup> )	Concrete Area in Shear Planes per Unit Length (in <sup>2</sup> /in)	Maximum Midspan Moment (kip-in)
SC12GN	4x5	C	12	Greased	No	7.35	0.0766	269.5
SC12UN	4x5	C	12	Ungreased	No	7.35	0.0766	305.8
SC3GN	4x5	C	3	Greased	No	32.16	0.3350	395.7
SU3GN	4x5	U	3	Greased	No	39.61	0.4126	445.7
SO3GN	4x5	O	3	Greased	No	30.93	0.3221	314.5
SO2GN	4x5	O	2	Greased	No	46.83	0.4878	354.1
SC3UN	4x5	C	3	Ungreased	No	32.16	0.3350	422.0
SC3GR	4x5	C	3	Greased	Yes	32.16	0.3350	492.1
TC12GN	5x6	C	12	Greased	No	7.35	0.0766	340.8
TC12UN	5x6	C	12	Ungreased	No	7.35	0.0766	388.9
TC3GN	5x6	C	3	Greased	No	32.16	0.3350	440.7
TU3GN	5x6	U	3	Greased	No	39.61	0.4126	483.9
TO3GN	5x6	O	3	Greased	No	30.93	0.3221	408.3
TO2GN	5x6	O	2	Greased	No	46.83	0.4878	400.5
TC3UN	5x6	C	3	Ungreased	No	32.16	0.3350	452.3
TC3GR	5x6	C	3	Greased	Yes	32.16	0.3350	518.7

Table 5: End slip, horizontal shear and concrete connector stress for test specimens.

Specimen ID	End Slip at Max. Moment (in)	Max. Horizontal Shear Force (kips)	End Slip at Max. Horiz. Shear (in)	Area of Conc. in Shear Planes within 18 in. (in <sup>2</sup> )	Concrete Shear Stress (psi)
SC12GN	0.2303	10.29	0.0469	1.3783	-
SC12UN	0.2121	10.47	0.0431	1.3783	-
SC3GN	0.0712	24.49	0.0305	6.0302	2354
SU3GN	0.0393	30.09	0.0216	7.4273	2666
SO3GN	0.2800	17.81	0.0207	5.7984	1295
SO2GN	0.0225	24.01	0.0143	8.7805	1562
SC3UN	0.0500	28.62	0.0251	6.0302	-
SC3GR	0.0621	29.66	0.0581	6.0302	-
TC12GN	0.2555	8.68	0.0398	1.3783	-
TC12UN	0.1974	18.80	0.0214	1.3783	-
TC3GN	0.0592	27.31	0.0320	6.0302	3090
TU3GN	0.0529	32.79	0.0391	7.4273	3247
TO3GN	0.1294	21.78	0.0176	5.7984	2260
TO2GN	0.0672	26.88	0.0097	8.7805	2073
TC3UN	0.0640	29.61	0.0274	6.0302	-
TC3GR	0.0355	35.01	0.0360	6.0302	-

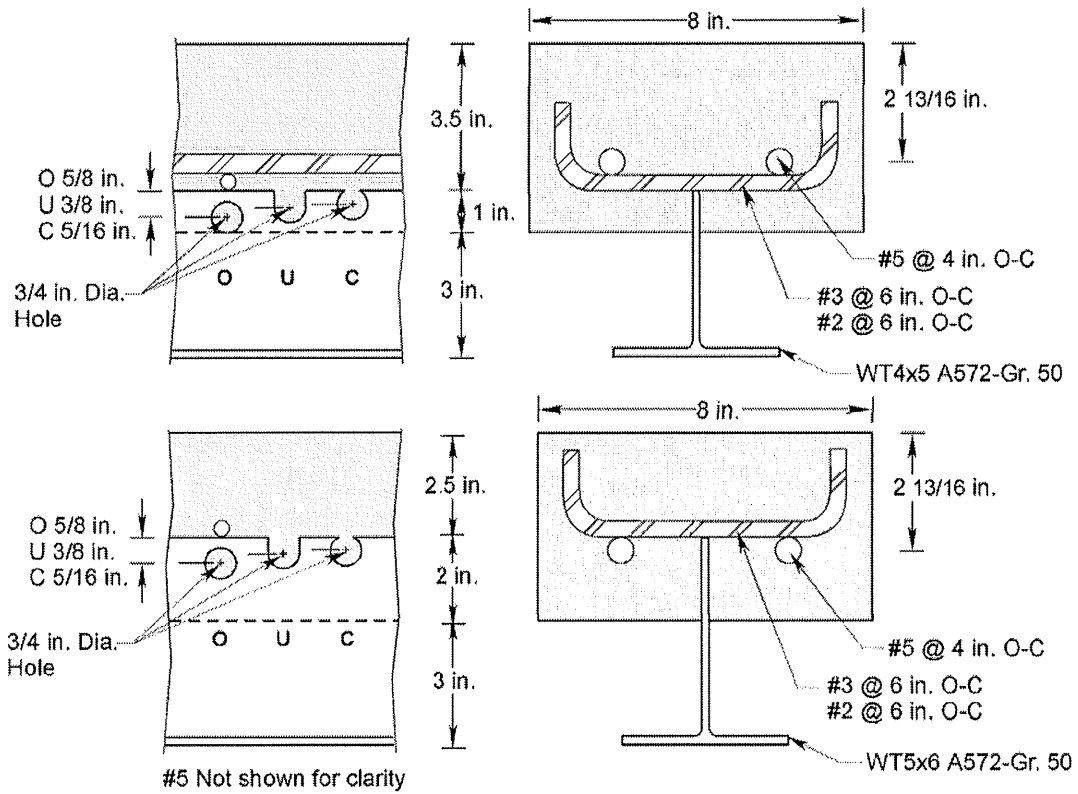


Fig. 1 – Specimen cross-sections.

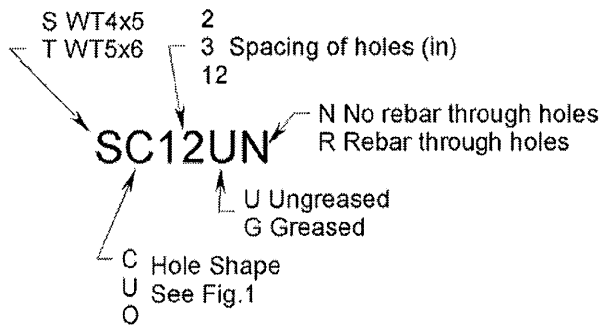


Fig. 2 – Specimen designation.



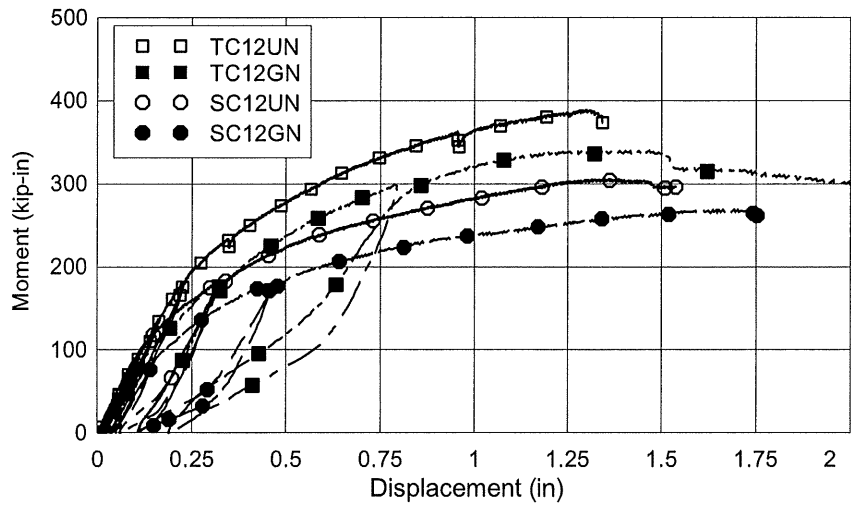


Fig. 4b – Moment-displacement response of specimens with widely spaced connectors and different web-concrete interfaces.

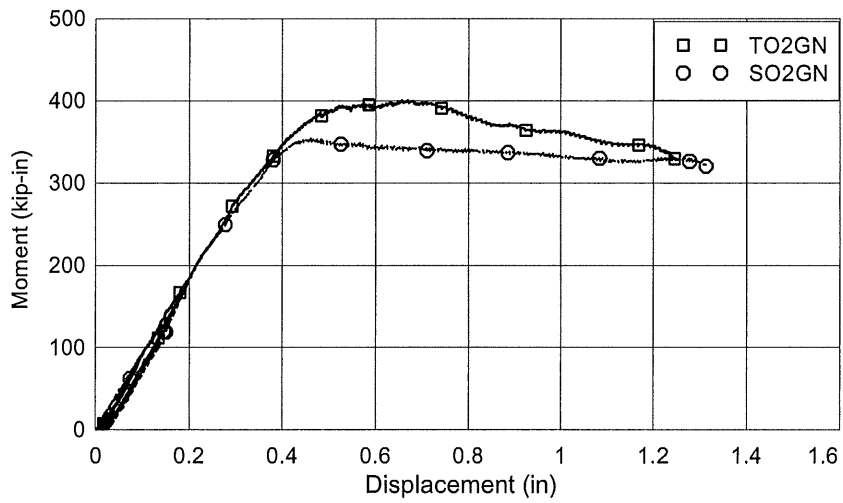


Fig. 4c – Moment-displacement response of specimens with different web-concrete embedment areas.

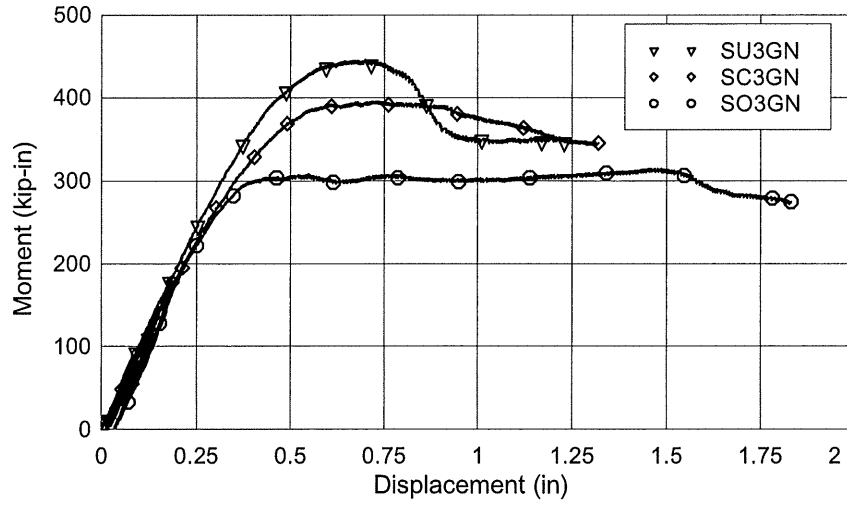


Fig. 4d – Moment-displacement response of specimens with different perforation shapes.

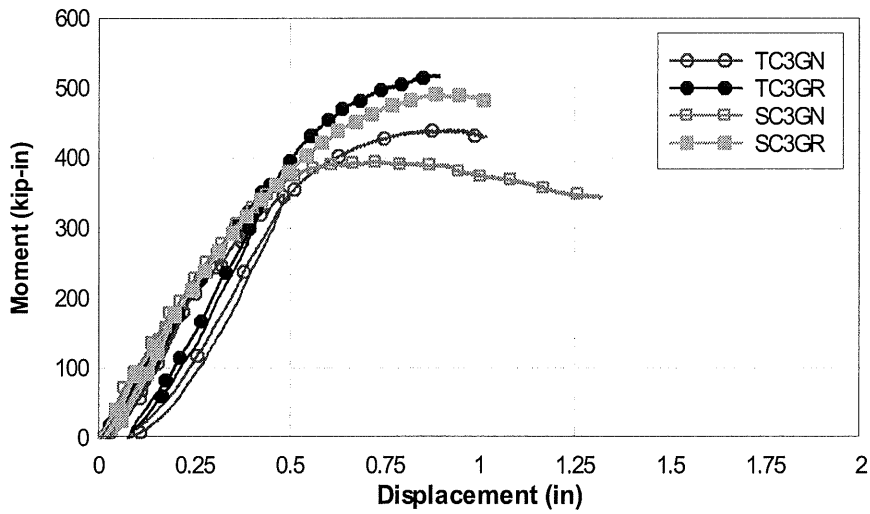


Fig. 4e – Moment-displacement response for WT4x5 and WT5x6 specimens with and without rebar through perforations.

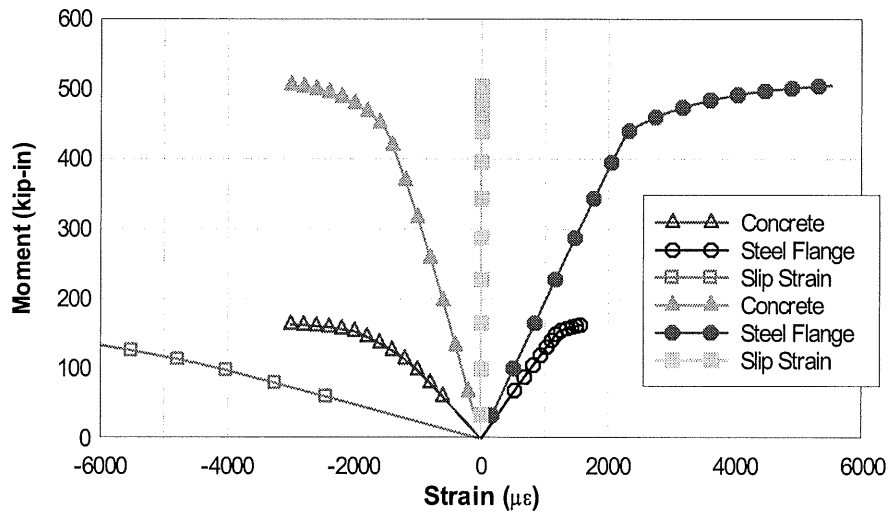


Fig. 5a – Theoretical strains on cross section for ideally composite and noncomposite sections (WT4x5 specimens).

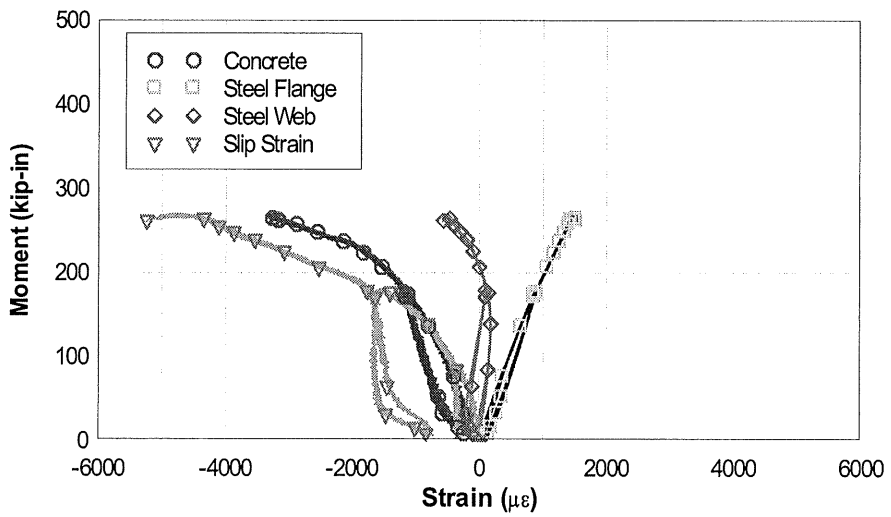


Fig. 5b – Strains at midspan of specimen SC12GN.

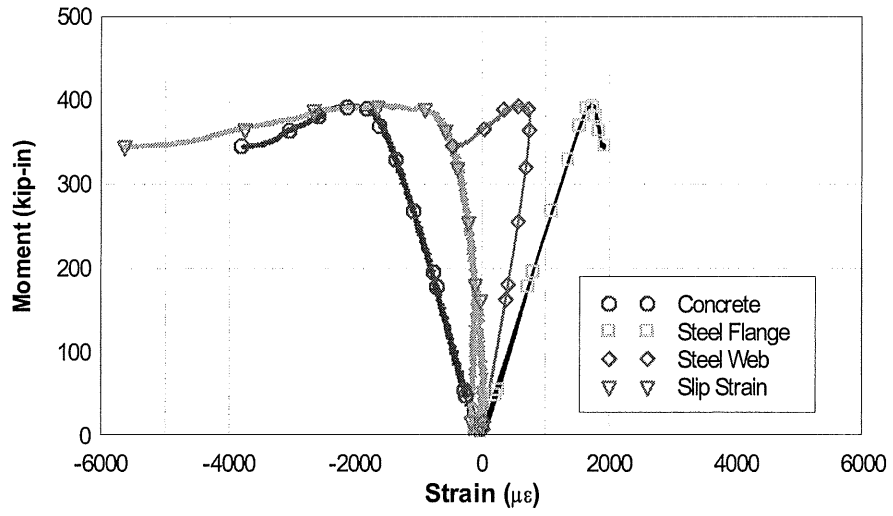


Fig. 5c – Strains at midspan of specimen SC3GN.

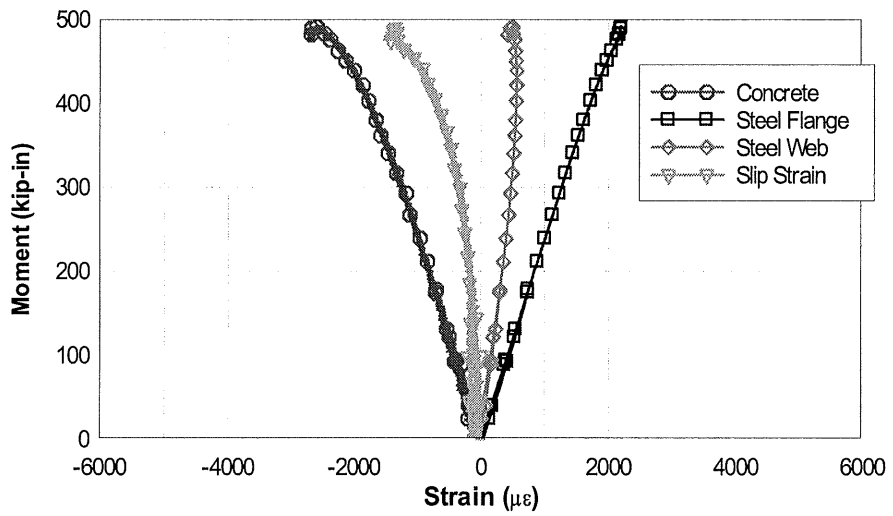


Fig. 5d – Strains at midspan of specimen SC3GR.

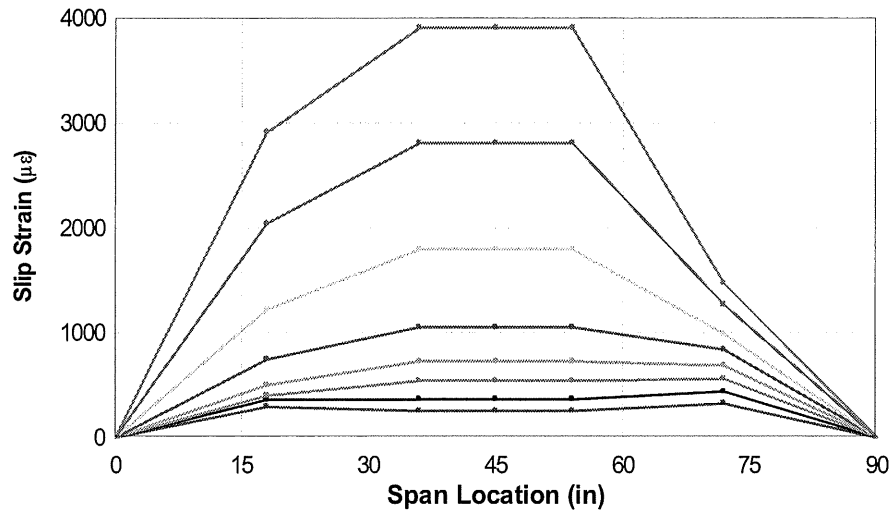


Fig. 6 – Slip strain distribution along beam for specimen SC3GN at increasing load amplitudes.

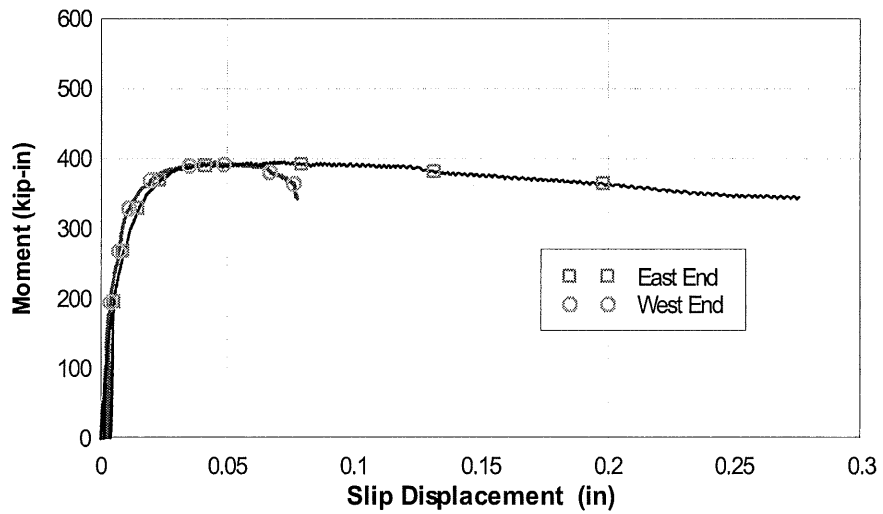


Fig. 7 – Relative displacement between steel web and concrete slab at end of specimen SC3GN.

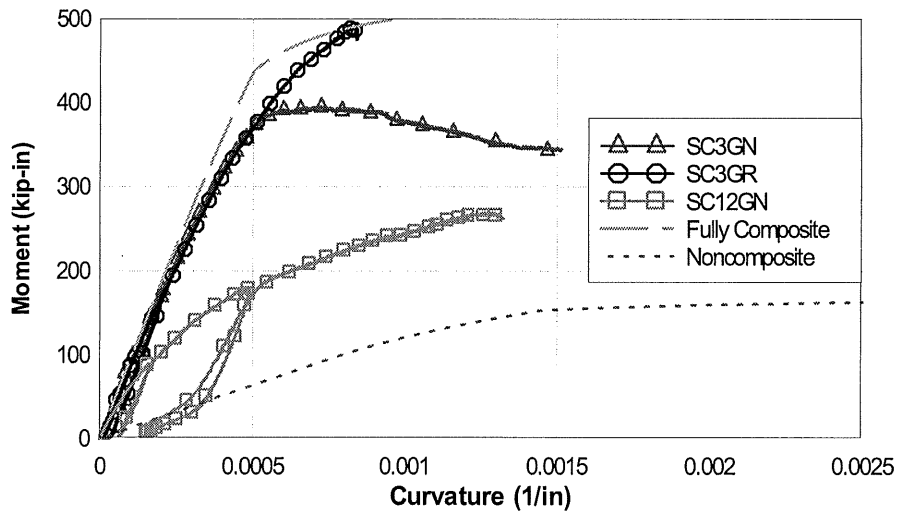


Fig. 8 – Moment-curvature responses for WT4x5 specimens with C-shaped perforations and theoretical behavior.

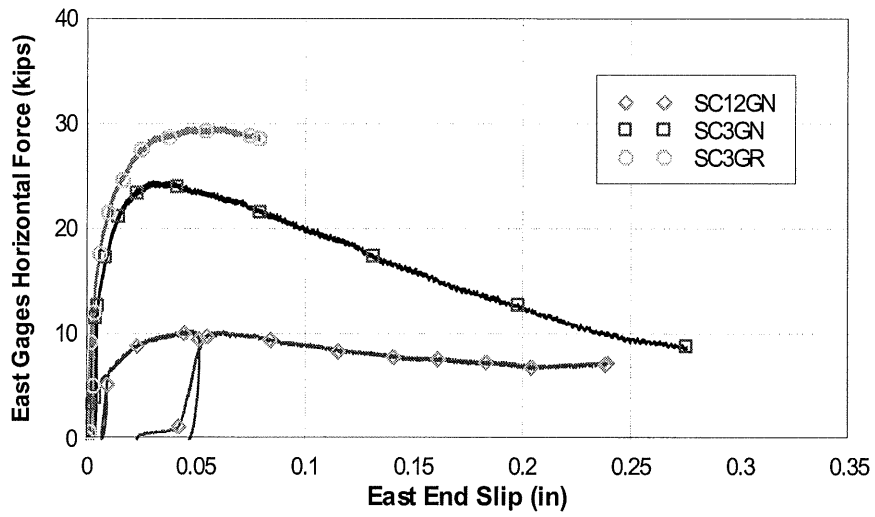


Fig. 9 – Horizontal shear force and end slip responses for WT4x5 specimens with C-shaped perforations on east side of specimen.

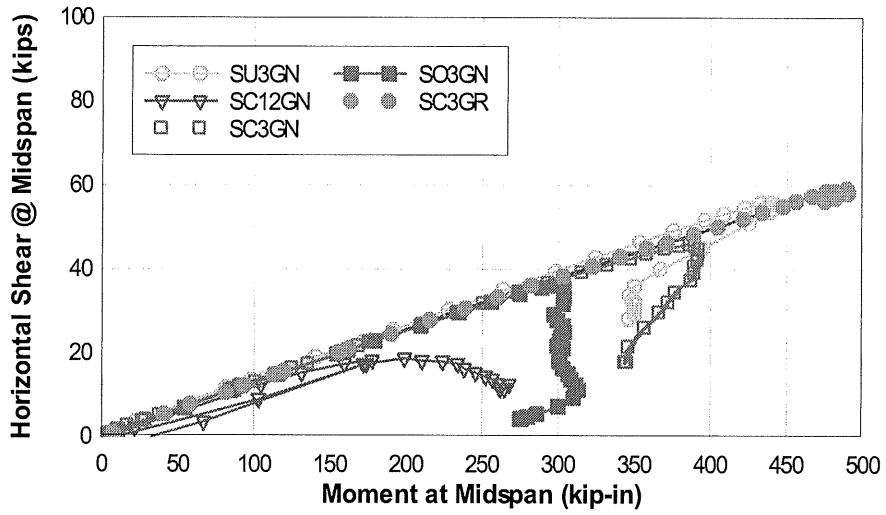


Fig. 10 – Horizontal shear force and applied moment at midspan for WT4x5 specimens.

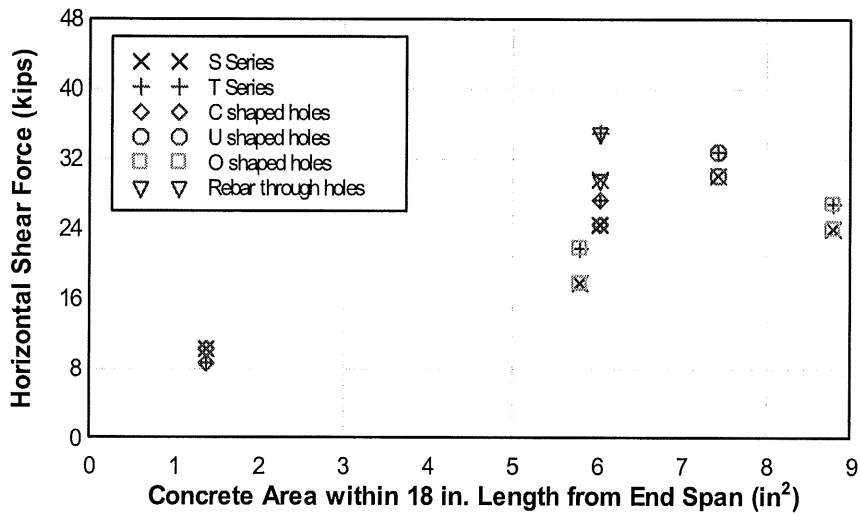


Fig. 11 – Horizontal shear force within first 18 in. from end of span for different perforations, steel web embedment areas, and rebar through the perforations.